Alterations of Choline Phospholipid Metabolism in Ovarian Tumor Progression

Egidio Iorio,[1] Delia Mezzanzanica,[2] Paola Alberti,[2] Francesca Spadaro,[1] Carlo Ramoni,[1] Sandra D'Ascenzo,[3] Danilo Millimaggi,[3] Antonio Pavan,[3] Vincenza Dolo,[3] Silvana Canevari,[2] and Franca Podo[1]

[1]Section of Molecular and Cellular Imaging, Department of Cell Biology and Neurosciences, Istituto Superiore di Sanità, Rome, Italy; [2]Unit of Molecular Therapies, Department of Experimental Oncology and Laboratories, Istituto Nazionale Tumori, Milan, Italy; and [3]Department of Experimental Medicine, University of L'Aquila, L'Aquila, Italy

Abstract

Recent characterization of abnormal phosphatidylcholine metabolism in tumor cells by nuclear magnetic resonance (NMR) has identified novel fingerprints of tumor progression that are potentially useful as clinical diagnostic indicators. In the present study, we analyzed the concentrations of phosphatidylcholine metabolites, activities of phosphocholine-producing enzymes, and uptake of [methyl-^{14}C]choline in human epithelial ovarian carcinoma cell lines (EOC) compared with normal or immortalized ovary epithelial cells (EONT). Quantification of phosphatidylcholine metabolites contributing to the ^{1}H NMR total choline resonance (3.20-3.24 ppm) revealed intracellular [phosphocholine] and [total choline] of 2.3 $\pm$ 0.9 and 5.2 $\pm$ 2.4 nmol/10^{6} cells, respectively, with a glycerophosphocholine/phosphocholine ratio of 0.95 $\pm$ 0.93 in EONT cells; average [phosphocholine] was 3- to 8-fold higher in EOC cells (P < 0.0001), becoming the predominant phosphatidylcholine metabolite, whereas average glycerophosphocholine/phosphocholine values decreased significantly to ≤0.2. Two-dimensional {phosphocholine/total choline, [total choline]} and {glycerophosphocholine/total choline, [total choline]} maps allowed separate clustering of EOC from EONT cells (P < 0.0001, 95% confidence limits). Rates of choline kinase activity in EOC cells were 12- to 24-fold higher (P < 0.03) than those in EONT cells (basal rate, 0.5 $\pm$ 0.1 nmol/10^{6} cells/h), accounting for a consistently elevated (5- to 15-fold) [methyl-^{14}C]-choline uptake after 1-hour incubation (P < 0.0001). The overall activity of phosphatidylcholine-specific phospholipase C and phospholipase D was also higher (~5-fold) in EOC cells, suggesting that both biosynthetic and catabolic pathways of the phosphatidylcholine cycle likely contribute to phosphocholine accumulation. Evidence of abnormal phosphatidylcholine metabolism might have implications in EOC biology and might provide an avenue to the development of noninvasive clinical tools for EOC diagnosis and treatment follow-up. (Cancer Res 2005; 65(20): 9369-76)

Introduction

Epithelial ovarian cancer (EOC) is the leading cause of death in women with gynecologic malignancies. Despite a relatively low morbidity, EOC presents a high case-fatality ratio and the overall 5-year survival is still <30% (1). Women with organ-confined tumors have an excellent prognosis, but the majority of early-stage cancers are asymptomatic or present nonspecific and variable clinical manifestations, frequently delaying disease diagnosis. Indeed, over two-thirds of patients are diagnosed with advanced disease (International Federation of Gynecology and Obstetrics stage III and IV; refs. 2, 3). Primary cytoreductive surgery followed by platinum-based chemotherapy is the standard treatment for this cancer. After a first high response rate, the patient usually relapses and the tumor becomes resistant to chemotherapy. Because EOC is intrapelvic, invasive methods are often unavoidable to monitor disease recurrence. Thus, there is a need for improved imaging methods to diagnose EOC and to monitor treatment response or tumor recurrence noninvasively.

The detection by nuclear magnetic resonance (NMR) of abnormal levels of choline phospholipid metabolites in tumor cells and tissues (reviewed in refs. 4–7) has recently led to pilot studies aimed at evaluating the clinical utility of *in vivo*–localized NMR spectroscopy (MRS) and radiolabeled choline-based positron emission tomography (PET) in human cancers, such as gliomas, breast, prostate, and gynecologic carcinomas (8–11). However, clinical application of imaging methods based on detection of choline metabolites awaits further elucidation of the relationships between specific biochemical features and tumor progression *in vitro* and *in vivo*.

High-resolution NMR methods provide powerful means to fill this basic knowledge gap, by measuring steady-state levels and fluxes of metabolites in the pathways responsible for biosynthesis and catabolism of phosphatidylcholine, the major phospholipid of eukaryotic cell membranes (Fig. 1). Substantially modified ^{1}H MRS spectral profiles have, in fact, been reported in the 3.20 to 3.24 ppm region (typical of trimethylammonium head groups of phosphatidylcholine precursors and catabolites, such as phosphocholine, glycerophosphocholine, and free choline) in malignant transformation of human mammary (12, 13) and prostate epithelial cells (14). In particular, increases in the levels of phosphocholine and "total choline–containing" (water-soluble) metabolites (total choline) have been reported in tumor cells together with decreases in the glycerophosphocholine/phosphocholine ratio (a phenomenon known as the "glycerophosphocholine-to-phosphocholine switch"; refs. 6, 12).

To date, choline phospholipid metabolism in ovarian cancer has received only limited attention despite preliminary indications of increased total choline in human ovary tumors and biopsies (15, 16) and accumulation of phosphocholine in ovarian carcinoma cell lines (17). In the present study, we quantified the intracellular levels of phosphatidylcholine metabolites in the progression from

Note: E. Iorio and D. Mezzanzanica contributed equally to this work.

Requests for reprints: Franca Podo, Department of Cell Biology and Neurosciences, Istituto Superiore di Sanità, Viale Regina Elena 299, 00161 Rome, Italy. Phone: 39-6-49902686; Fax: 39-6-49387144; E-mail: fpodo@iss.it.

doi:10.1158/0008-5472.CAN-05-1146

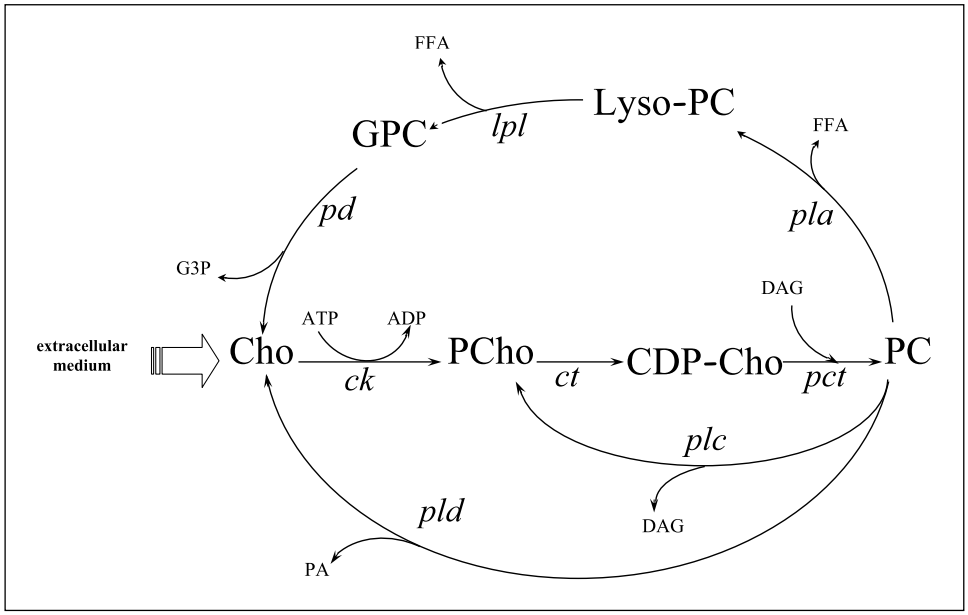

Figure 1. Schematic representation of phosphatidylcholine (*PC*) *de novo* biosynthesis and catabolism. Metabolites: *CDP-Cho,* CDP choline; *Cho,* choline; *DAG,* diacylglycerol; *FFA,* free fatty acid; *G3P,sn*-glycerol-3-phosphate; *GPC,* glycerophosphocholine; *PA,* phosphatidate; *PCho,* phosphocholine. Enzymes: *ck,* choline kinase (EC 2.7.1.32); *ct,* cytidylyltransferase (EC 2.7.7.15); *lpl,* lysophospholipase (EC 3.1.1.5); *pct,* phosphocholine transferase (EC 2.7.8.2); *pd,* glycerophosphocholine phosphodiesterase (EC 3.1.4.2); *pla,* phospholipase A_2 (EC 3.1.1.4) and phospholipase A_1 (EC 3.1.1.32); *plc,* phospholipase C (EC 3.1.4.3); *pld,* phospholipase D (EC 3.1.4.4).

nontumoral ovarian surface epithelial (OSE) cells or immortalized cell variants to ovarian cancer cell lines and related these levels to quantitative differences in basal activity of enzymes involved in phosphatidylcholine biosynthesis and/or catabolism (see Fig. 1). In particular, the choline kinase basal activity rate and the overall phosphatidylcholine-specific phospholipase C (PLC) and phospholipase D (PLD) activity were evaluated. The effects of altered phosphatidylcholine metabolism led to a difference between intact tumor and nontumor cells in [methyl-^{14}C]choline uptake and subsequent ^{14}C-label release into the medium.

Materials and Methods

Epithelial ovarian nontumoral and carcinoma cells. OSE cells were scraped from the surface of normal human ovaries obtained at surgery for benign or malignant gynecologic diseases other than ovarian carcinoma. All human materials were obtained with informed consent from patients. OSE cells were maintained in culture for three to five passages in a 1:1 (v/v) ratio of MCDB-105/Medium-199 (Sigma, St. Louis, MO) supplemented with 15% FCS (Sigma, St. Louis, MO) and 100 μg/mL gentamicin, and their origin was confirmed by immunohistochemical assay for expression of cytokeratin-8/18 and vimentin, essentially as described (18). Life span of short-term cultures of OSE cells was increased up to 15 to 16 passages by SV40 large T antigen transfection, thus obtaining immortalized OSE (IOSE) cells. Stably IOSE cells were obtained by transfection with the cDNA of the catalytic subunit of the human telomerase reverse transcriptase (hTERT; kindly provided by Dr. R.A. Weinberg, Whitehead Institute, Cambridge, MA), thus obtaining hTERT cells. Both IOSE and hTERT cells were maintained in the same medium as OSE cells. The following human serous ovarian carcinoma cell lines were used: IGROV1 (ref. 19; a gift from J. Benard, Institute Gustave Roussy, Villejuif, France); OVCAR3 (20) and SKOV3 (obtained from the American Type Culture Collection, Manassas, VA; ref. 21); OVCA432 (kindly provided by R. Knapp, Dana-Farber Institute, Boston, MA; ref. 22); and CABA I (established from the ascitic fluid of a patient with ovarian carcinoma before any drug treatment; ref. 23). All EOC lines were of ascitic origin, except IGROV1, which derived from primary adenocarcinoma.

Tumor cell lines were maintained in RPMI 1640 (Sigma, St. Louis, MO) supplemented with 10% (v/v) FCS and 2 mmol/L L-glutamine (Sigma, St. Louis, MO). All cells were cultured in a humidified atmosphere of 5% CO_2 at 37°C and routinely tested for *Mycoplasma* infection using the *Mycoplasma* PCR ELISA kit (Roche, Basel, Switzerland).

Optical microscopy analyses and biochemical assays showed that cell sizes and protein contents were not significantly different between EOC and epithelial ovarian nontumoral (EONT) cells. In particular, cell volumes, measured as described already (12), presented quite broad distribution ranges for both cell types, with average values of $1.9 \pm 0.7 \times 10^3$ μm^3 for EOC and $2.4 \pm 1.4 \times 10^3$ μm^3 for EONT cells.

Cell extracts in aqueous phase. Cells grown to 60% to 70% confluence were trypsinized 24 hours after culture medium change, counted, and assessed for viability (80-90%) and membrane integrity by trypan blue staining. Cells were washed twice with ice-cold physiologic saline solution and pellets resuspended in 0.5 mL ice-cold twice-distilled water. Aqueous extracts (20×10^6-30×10^6 cells/sample) were prepared in ethanol/H_2O (70:30, v/v) according to an established protocol already described (17, 24, 25). This method was proven to be as efficient as the more commonly used extraction in perchloric acid, with the additional advantages of higher procedural simplicity (26, 27). Samples were ultrasonicated at 20 kHz with an exponential probe, 8 μm peak-to-peak by a MSE ultrasonic disintegrator Mk2 (Crawley, Sussex, United Kingdom) and centrifuged at 14,000 × *g* for 30 minutes. Supernatants were lyophilized twice in a RVT 4104 Savant lyophilizer (Mildford, ME), and the residue was resuspended in 0.7 mL D_2O (Sigma-Aldrich, Milan, Italy) containing 0.1 mmol/L TSP as internal standard (Merck & Co., Montreal, Quebec, Canada).

Nuclear magnetic resonance spectroscopy. High-resolution NMR experiments (25°C) were done at either 400 or 700 MHz (Bruker AVANCE spectrometers, Karlsruhe, Germany). ^{1}H NMR spectra of cell extracts were obtained using acquisition pulses, water presaturation, data processing, and data analysis as described already (17). Quantification of individual metabolites was obtained from peak areas using correction factors determined by experiments at the equilibrium of magnetization (90° pulses, 30.00-second interpulse delay). In some samples, parallel ^{31}P NMR experiments were also done at 161.97 MHz as described previously (24) to verify by an independent method phosphocholine and glycerophosphocholine contents from peak areas of the respective signals at 3.78 and 0.49 ppm. The values of absolute metabolite concentrations obtained by the two methods were fully consistent and pooled together. Metabolite quantification was expressed as nanomoles and normalized to the number of extracted cells (and also converted into fmol/μm^3 cell volume, for comparison with other cell systems).

Nuclear magnetic resonance assays of basal choline kinase activity. Cells (40×10^6) were homogenized at ice melting temperature in a Potter homogenizer in the presence of 4 volumes of 100 mmol/L Tris-HCl (pH 8.0) containing 10 mmol/L DTT and 1 mmol/L EDTA in D_2O.

The homogenate was further disrupted at 0°C by ultrasonication at 20 KHz with an exponential probe, 8 μm peak-to-peak, for two time periods of 30 seconds each, centrifuged at 20,000 × *g* for 30 minutes, and the supernatant (cytosolic preparation) was transferred to a NMR tube. Basal choline kinase activity rate was assayed at 25°C on addition of exogenous choline chloride, ATP, and Mg^{2+} ions in Tris-HCl buffer (to final concentrations of 5 mmol/L choline, 10 mmol/L ATP, and 10 mmol/L $MgCl_2$). Substrate and product concentrations were simultaneously measured from the ^{1}H NMR peak areas (corrected for the respective factors of partial saturation of the magnetization vector). Choline kinase activity was determined by linear regression analysis of data points in the linear portion (10-60 minutes, correlation coefficient R^2 between 0.97 and 0.99) of the curve representing the time course of phosphocholine production during the reaction done in excess of substrate (ref. 28 and references therein) using GraphPad Software version 3.03 (GraphPad Software, Inc., San Diego, CA). The rate of linear phosphocholine production essentially coincided with that of choline consumption in the same time interval, indicating no major interference from other reactions competing for substrate or product utilization (a major concern in conventional colorimetric/enzymatic assays on cell lysates). Independent ^{31}P NMR analyses (25), done on EOC samples in the same time interval and with comparable time resolution (15-60 minutes, R^2 = 0.92-0.99), confirmed the values of choline kinase rates determined by ^{1}H NMR. For these samples, the results obtained by the two techniques were therefore combined.

Fluorimetric assay of phosphatidylcholine-specific phospholipase C and phospholipase D. The overall activity of phosphatidylcholine-specific PLC and PLD was determined using the Amplex Red phosphatidylcholine-specific PLC assay kit (Molecular Probes, Inc., Eugene, OR) according to described procedures adapted to enzymatic analysis of total cell lysates (29). Briefly, egg yolk phosphatidylcholine was used as substrate. Phosphocholine produced by phosphatidylcholine-PLC–mediated phosphatidylcholine hydrolysis was converted into choline by alkaline phosphatase. Total choline was then measured by conversion into betaine and H_2O_2 (by choline oxidase) and subsequent reaction of H_2O_2 with Amplex Red reagent (10-acetyl-3,7-dihydrophenoxazine) in the presence of horseradish peroxidase to generate the fluorescent probe resorufin. Fluorescence (560 ± 5 nm excitation, 590 ± 10 nm emission) was measured by a Perkin-Elmer LS-50B spectrofluorimeter (Perkin-Elmer Ltd., Beaconsfield, Buckinghamshire, United Kingdom).

[^{14}C]choline uptake assay. For each cell line, 5×10^5 cells per well were seeded in two parallel experiments (each in triplicate) in a six-well plate in 2 mL complete medium and left to adhere for 24 hours at 37°C. Exponentially growing cells were pulsed for 1 hour with 0.02 μCi [methyl-^{14}C]choline chloride per well (Amersham Biosciences, Little Chalfont, United Kingdom) at 37°C and extensively washed twice with PBS. Cells from one series of triplicates were completely solubilized and harvested by adding 0.5 mL of 0.25 N NaOH (Sigma, St. Louis, MO). Cell-associated radioactivity due to [methyl-^{14}C]choline uptake [^{14}C-UPT (1 hour)] was determined by scintillation counting after addition of 2.5 mL Optiphase Super Mix scintillation cocktail (Perkin-Elmer Life Science). After washes in PBS, cells from the second series of triplicates were further incubated for 24 hours at 37°C in fresh medium, washed again with PBS and solubilized as described above, and subjected to scintillation counting. This assay measured the overall radioactivity still associated with cellular compartments 24 hours after the 1-hour pulse with radiolabeled choline [^{14}C-RET (24 hours)]. For each radiolabeled series of cells, a parallel set of experiments with unlabeled cells was used for cell number counting after trypsinization (0.5 mL for 5 minutes). The percentage of ^{14}C-label released into the medium over 24 hours [^{14}C-REL (24 hours)] was calculated from scintillation counts obtained after the 1-hour [^{14}C]choline pulse and after the 24-hour chase (normalized to the respective cell numbers) as follows:

$$^{14}\mathrm{C}-\mathrm{REL}\,(24\,\mathrm{h}) = [^{14}\mathrm{C}-\mathrm{UPT}\,(1\,\mathrm{h}) - {}^{14}\mathrm{C}-\mathrm{RET}\,(24\,\mathrm{h})]/{}^{14}\mathrm{C}-\mathrm{UPT}(1\,\mathrm{h})$$

Statistical analysis. Data were analyzed using GraphPad Software version 3.03. Statistical significance of differences was determined by one-way ANOVA or by Student's *t* test as specified. Differences were considered significant at $P < 0.05$.

Results

Abnormal concentrations of phosphatidylcholine metabolites are detected in ovarian cancer cells. One-dimensional ^{1}H NMR spectra on aqueous extracts revealed a more intense total choline resonance in five EOC cell lines compared with normal (OSE) or immortalized (IOSE and hTERT) cells (Fig. 2*A*). Moreover, analysis of expanded total choline spectral profiles showed that the relative areas of signal components due to individual phosphatidylcholine metabolites (glycerophosphocholine, phosphocholine, and choline) changed in the progression from nontumor to carcinoma cells, with phosphocholine becoming predominant in all carcinoma cells tested (Fig. 2*B*). High-resolution NMR revealed no significant differences between extracts of normal OSE and IOSE (IOSE and hTERT) cells in absolute concentrations of individual phosphatidylcholine metabolites or in glycerophosphocholine/phosphocholine ratio (Fig. 3*A* and *B, left*); thus, the respective concentrations of individual phosphatidylcholine metabolites and the glycerophosphocholine/phosphocholine ratios determined in eight independent experiments on epithelial ovarian nontumor (EONT, normal plus immortalized) cells were averaged (mean ± SD), with the following results: [glycerophosphocholine] = 1.9 ± 1.4 nmol/10^6 cells, [phosphocholine] = 2.3 ± 0.9 nmol/10^6 cells, [choline] = 1.1 ± 1.1 nmol/10^6 cells, glycerophosphocholine/phosphocholine = 0.95 ± 0.93, and [total choline] = [glycerophosphocholine + phosphocholine + choline] = 5.2 ± 2.4 nmol/10^6 cells. The quite large scatter of some determinations could be attributed to the possible combination of several factors, including biological variability of cell cultures of OSE and their immortalized cell variants (derived from different individuals and analyzed at different passages), variability in the timing of cell harvest, and (to a lower extent) spectral deconvolution of overlapping peaks. In spite of data scatter, comparison of the average phosphocholine contents in EONT cells with those in EOC cells (Fig. 3*A, right*) revealed a 3- to 8-fold increase in the average content of this metabolite in all EOC cells ($P < 0.0001$). The same level of statistical significance was maintained when phosphocholine contents were normalized to the respective cell volumes (1.3 ± 0.9 fmol/μm^3 cell in EONT and 3- to 10-fold higher values in the whole set of carcinoma cells). No significant differences ($P > 0.05$) were found between the levels of phosphatidylcholine metabolites in individual EOC cell lines (all possessing highly malignant phenotypes), although a lower average phosphocholine content was measured in SKOV3, the only cell line exhibiting mixed mesenchymal/epithelial characteristics. Consistent with the elevation in [phosphocholine] content, the average pool size of total choline also increased (2.0- to 4.4-fold) in all EOC cells ($P < 0.0001$), whereas the average glycerophosphocholine/phosphocholine ratio declined to values between 0.01 and 0.12 ($P < 0.01$). The latter finding is in general agreement with the glycerophosphocholine-to-phosphocholine switch described for other types of cancer or oncogene-transformed cells (6, 12).

The data above showed a significant modification not only in [total choline] but also in the relative contributions of phosphocholine and glycerophosphocholine to the total choline pool in EOC cells. In fact, the average phosphocholine/total choline

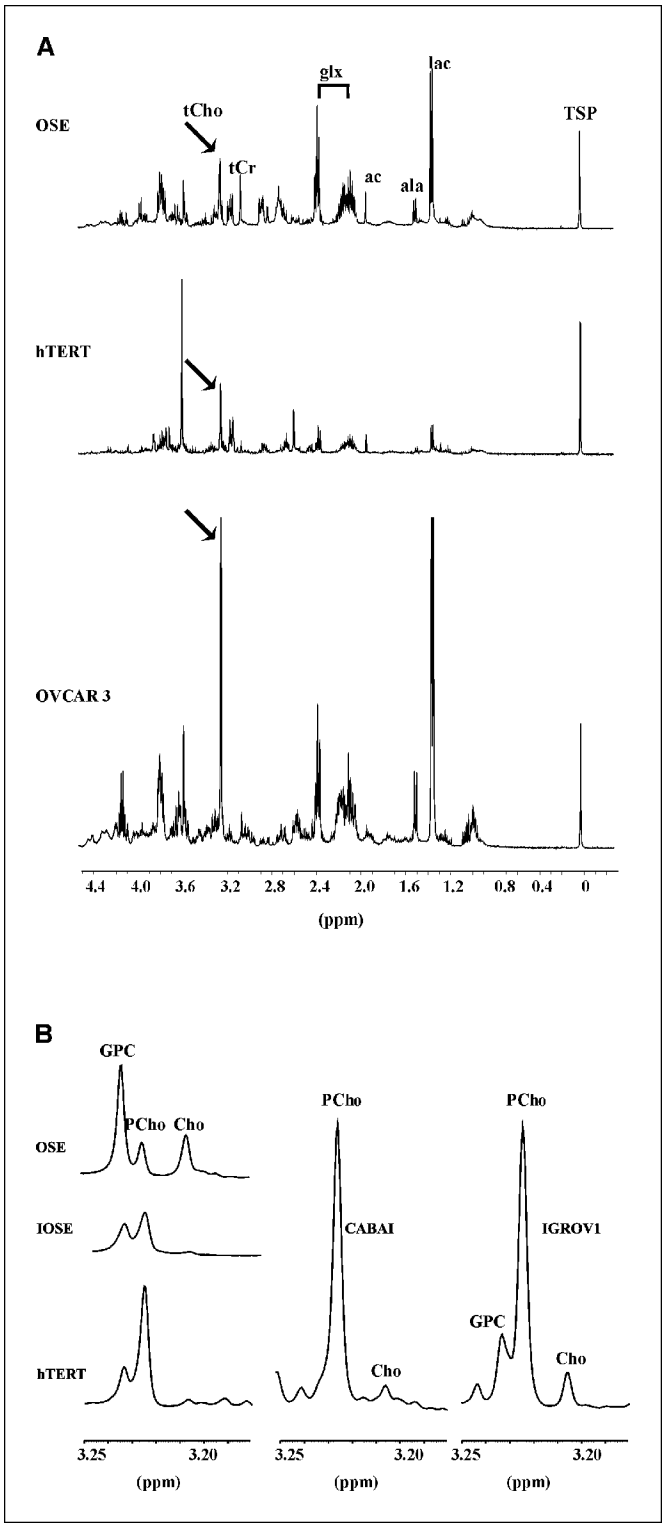

Figure 2. Representative ^{1}H NMR spectra of aqueous extracts of ovary epithelial nontumor and tumor cells. *A,* spectra (400 MHz) of normal OSE (1st-2nd passage), immortalized cell variant hTERT (39th passage) and OVCAR3 ovarian carcinoma cells. *Arrows,* resonance band of trimethylammonium moieties of total choline (*tCho*)–containing metabolites (3.20-3.24 ppm). Other peak assignments: *tCr,* total creatine (creatine + phosphocreatine); *glx,* glutamate + glutamine; *ac,* acetate; *ala,* alanine; *lac,* lactate; *TSP,* internal reference signal. *B,* expanded ^{1}H NMR spectral profiles (700 MHz) of total choline in aqueous extracts of normal OSE (3rd passage), IOSE (16th passage), and hTERT (52nd passage) cells and two ovarian carcinoma cell lines (CABA I and IGROV1).

increased from 0.49 ± 0.19 in EONT to 0.70 ± 0.89 in EOC cells, with a parallel decrease in the average glycerophosphocholine/total choline from 0.34 ± 0.10 to <0.11.

To further evaluate the role of [phosphocholine] and glycerophosphocholine/phosphocholine ratio in discriminating the biochemical behavior of EOC from EONT cells, two-dimensional maps were constructed by plotting either the phosphocholine/total choline or the glycerophosphocholine/total choline ratio versus [total choline] for all sets of experimental data (Fig. 4). These analyses allowed clear-cut separation of EOC from EONT cells into independent clusters ($P < 0.0001$ on both axes). In fact, EONT data were confined within areas characterized by an upper [total choline] value of 7.00 nmol/10^6 cells, an upper phosphocholine/total choline value of 0.65, and a lower glycerophosphocholine/total choline value of 0.25 (95% confidence limits). The corresponding variables measured for EOC cells were outside these thresholds (Fig. 4, *dashed lines*), with total choline contents extending from 7.4 to 32.5 nmol/10^6 cells, the phosphocholine/total choline ratio ranging between 0.68 and 0.98, and the glycerophosphocholine/total choline ratio between 0.20 and <0.01.

The observed modifications in the levels of intracellular phosphatidylcholine metabolites in EOC with respect to EONT cells could not be simply attributed to different cell doubling time, which was 41 ± 8 hours for all cell systems analyzed, with the exception of OSE cells, which had an estimated doubling time of ~5 days. Nevertheless, this difference did not lead to any separation of OSE cell data outside the clusters typical of EONT cells (Fig. 4).

Enzymes responsible for phosphocholine production are activated in ovarian cancer cells. Major contributions to phosphocholine accumulation may derive from alternative or combined activation of enzymes involved in phosphatidylcholine biosynthesis and/or catabolism (see Fig. 1), notably choline kinase (responsible for choline phosphorylation in the Kennedy pathway), phosphatidylcholine-PLC (responsible for phosphatidylcholine hydrolysis into phosphocholine and diacylglycerol), and PLD (whose product, choline, may in turn be converted into phosphocholine by choline kinase). Thus, enzymatic assays were done to assess whether and to what extent these enzymes were activated in carcinoma cells.

The activity rate of choline kinase was measured by NMR assay in cytosolic cell preparations of EONT and four EOC cell lines. Because this assay requires a large number of cells, hTERT cells were used to represent the EONT group. Figure 5*A* shows a typical example of the time course of choline kinase–mediated net phosphocholine production and choline consumption, as determined from the area of the corresponding ^{1}H NMR signal in CABA I cytosolic preparations (*left*), and representative experiments to assess choline kinase activity rates in hTERT and EOC cells (*right*). Two independent series of ^{1}H NMR experiments were carried out to determine the basal choline kinase activity in hTERT cells. In view of the much higher levels of phosphocholine formed during the reaction in EOC cell preparations, the kinetics of choline phosphorylation could also be effectively monitored in these samples by ^{31}P MRS (two independent experiments on OVCAR3 and one for each of the other cell lines). ^{1}H and ^{31}P NMR gave consistent results. As reported in Fig. 5*B*, these assays revealed an average basal choline kinase rate of 0.5 ± 0.1 nmol/10^6 cells/h in hTERT cells and a significant increase to 12- to 24-fold higher values in the overall set of EOC cells ($P = 0.027$).

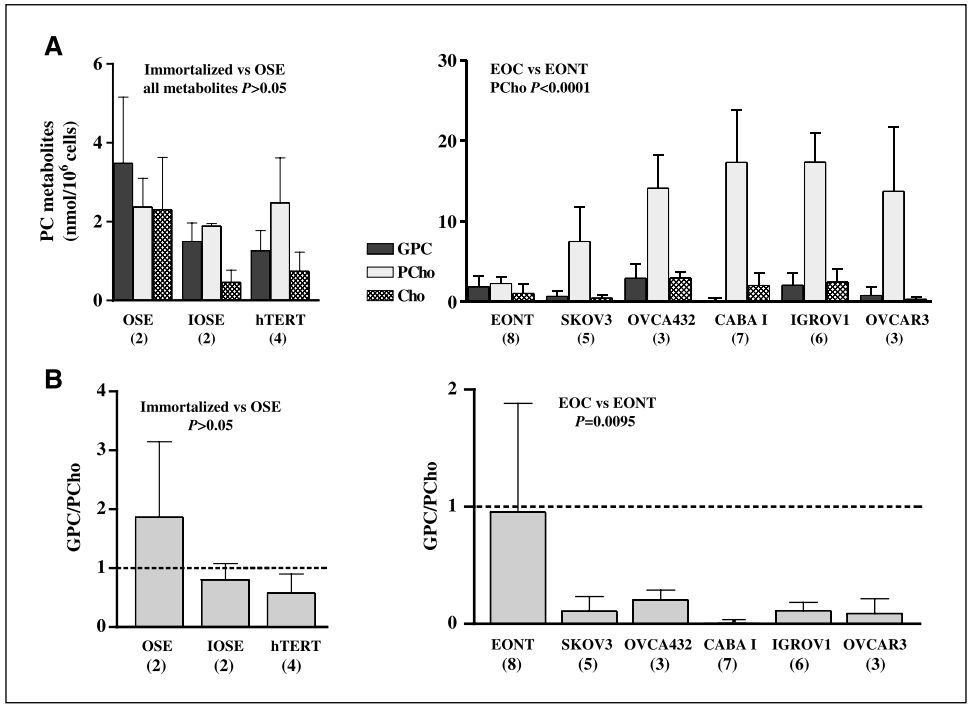

Figure 3. Intracellular concentrations of phosphatidylcholine metabolites determined by ^{1}H and ^{31}P NMR analyses of aqueous extracts of ovarian normal, immortalized, and cancer cells. *A,* glycerophosphocholine, phosphocholine, and choline in OSE (1st-3rd passages), immortalized IOSE (16th and 17th passages), immortalized hTERT (17th, 39th, and 52nd passages) cells and carcinoma cell lines (SKOV3, OVCA432, CABA I, OVCAR3, and IGROV1). The number of independent experiments done for each cell type is indicated in parentheses. Because no statistically significant difference ($P > 0.05$) was found for any phosphatidylcholine metabolite (glycerophosphocholine, phosphocholine, or choline) measured in immortalized cells (IOSE and hTERT) with respect to normal OSE cells (*left*), the average $\pm$ SD content of each metabolite was calculated by pooling data obtained for the overall set of EONT cells analyzed (*right*). The difference in [phosphocholine] between the overall set of EOC and EONT cells analyzed was statistically significant ($P < 0.0001$, one-way ANOVA). *B,* glycerophosphocholine/phosphocholine ratio in OSE, IOSE, hTERT, and EOC cells (same samples and statistical analysis as in *A*). Note the different scales in the *Y axis* of *left* and *right histograms*. *Bars,* half-maximum deviation for $n = 2$ and SD for $n \geq 3$.

Fluorimetric evaluation of overall phosphatidylcholine-PLC/PLD activity (measured in total cell lysates, without discriminating single enzyme activities) also revealed a 4.8- to 6.4-fold increase in EOC compared with EONT cells (Fig. 5*C*).

Together, the results of all enzymatic assays indicated that activation of enzymes involved in both biosynthetic and catabolic pathways of the phosphatidylcholine cycle can contribute to the increased phosphocholine levels measured in EOC compared with EONT cells.

[^{14}C]choline uptake increases in ovarian cancer cells. Intracellular trapping of choline transported into cells occurs through choline kinase–mediated phosphorylation of choline and subsequent accumulation of phosphocholine, which in turn acts as substrate for further enzymatic steps leading to phosphatidylcholine biosynthesis. To better evaluate the relevance of increased choline kinase activity observed in cancer cells, the uptake of [methyl-^{14}C]choline was measured in intact normal, immortalized (IOSE and hTERT), and carcinoma cell lines after 1-hour incubation with the radiolabeled substrate. In this time interval, the ^{14}C-label transported into the cell is expected to redistribute mostly among water-soluble metabolites of the Kennedy pathway (see Fig. 1), with only limited incorporation into choline-containing phospholipids (30–32). No significant differences between immortalized and normal cells were found in the specific scintillation counting (cpm/10^5 cells; Fig. 6, *left*), so that ^{14}C-label uptake in the overall series of EONT cells was averaged and compared with that in carcinoma cell lines (Fig. 6, *right*). The mean cellular radiolabel incorporation was 5- to 15-fold higher in cancer cells and the difference between the overall series of EOC lines and EONT cells was significant ($P < 0.0001$).

Furthermore, the percentage of ^{14}C-label released into the medium in the subsequent 24 hours of incubation in [^{14}C]choline-free medium was higher ($P = 0.05$) in EOC cells (63.3 $\pm$ 9.2%) than in EONT cells (45.5 $\pm$ 11.4%). These results are generally consistent with the observed overall activation of phosphatidylcholine-specific phospholipases in EOC cells. In fact, previous studies on radioactive choline-labeled, stimulated HeLa cells (30) or fibroblasts (31, 33) showed that the rate of label release into the medium increased over 2-fold on cell stimulation, and involved phosphatidylcholine metabolites not exclusively derived from cytosolic pools (nor from sphingomyelin), mainly occurring (for >80%) under the form of phosphocholine. Rapid protein kinase C–dependent activation of membrane-associated phosphatidylcholine-specific phospholipases was therefore suggested to be a prevalent mechanism of label release to the medium, with respect to passive export of phosphatidylcholine metabolites.

Discussion

Abnormal phosphatidylcholine metabolism is reported as a common feature in breast and prostate cancer cell lines, with consequent alterations in the levels of NMR-detectable compounds, such as phosphocholine and total choline, and in the glycerophosphocholine/phosphocholine ratio (4–7). In those experimental models, spectral changes did not correlate with cell doubling times; thus, these signals were proposed as fingerprints of tumor progression and/or end points of therapeutic treatment (7, 12–14, 34).

We show here, for the first time, that quantitative alterations in intracellular levels of phosphocholine, as well as the activation of both biosynthetic (choline kinase) and catabolic (phosphatidylcholine-PLC/PLD) enzymes involved in intracellular phosphocholine production, occur during ovary cancer progression. Intracellular concentrations of phosphocholine in EOC cells reached average values of 7.5 to 17.3 nmol/10^6 cells (3.6-12.7 fmol/μm^3). These levels were 3- to 8-fold higher in EOC relative to EONT cells. These average phosphocholine contents are among the highest thus far reported for human epithelial tumor cells, such as highly metastatic breast or prostate carcinoma cell lines (for which values up to 4.0 fmol/μm^3 have been reported; refs. 12, 14).

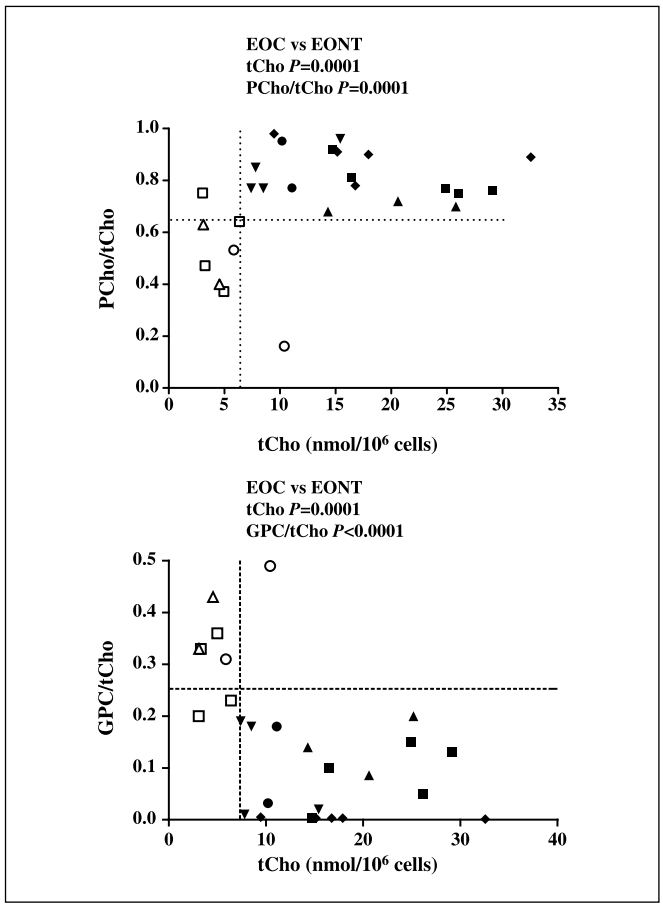

Figure 4. Clustering of EOC [OVCAR3 (●), IGROV1 (■), CABA I (♦), SKOV3 (▼), and OVCA432 (▲)] and EONT [OSE (○), IOSE (△), and hTERT (□)] cell data in separate areas of two-dimensional {phosphocholine/total choline, [total choline]} and {glycerophosphocholine/total choline, [total choline]} metabolic maps. *Dashed lines,* borders of EONT clustering areas constructed using the upper 95% confidence limit for [total choline], the upper 95% confidence limit for phosphocholine/total choline, and the lower 95% confidence limit for glycerophosphocholine/total choline values.

Moreover, phosphocholine represented the major fraction (>70%) of the total choline resonance of EOC cells and thus accounted mainly for the increase in [total choline] and decrease in the glycerophosphocholine/phosphocholine occurring in tumor versus nontumor cells.

These biochemical modifications did not correlate with the cell doubling time of ovarian carcinoma cells, arguing against the role of such changes as simple indicators of enhanced cancer cell proliferation. This body of evidence supports the general hypothesis that the multiple genetic changes occurring during carcinogenesis, and the associated alterations in growth factor–mediated cell signaling pathways, may ultimately result in induction or down-regulation of enzymes involved in the phosphatidylcholine cycle (see Fig. 1).

These aspects seem particularly interesting in view of current efforts in molecular therapeutics and pharmacogenomics aimed at identifying new targets that may be relatively specific for growth, progression, and survival of ovarian cancer (35). Signal transduction pathways triggered by tyrosine kinase receptors and/or controlled by oncogenes or intracellular protein kinases (such a Ras, Raf-1, mitogen-activated protein kinase, and extracellular signal-regulated kinase-1/2), activity of cyclic AMP–dependent protein kinase A, and signaling through phospholipid growth factors, such as lysophosphatidic acid (35–38), have been reported to be related to phosphatidylcholine metabolism deregulation at the level of either choline kinase (39–41) and/or phosphatidylcholine-specific phospholipases (42–44). Although most of the above-mentioned signaling alterations have been also recorded in some of the EOC lines used in our study, no specific investigations have been thus far done on their relationships with aberrant phosphatidylcholine metabolism. Regarding the biosynthetic phosphatidylcholine pathway, choline kinase is known to exert a primary influence on phosphocholine levels. The present provided evidence of a 12- to 24-fold increase in choline kinase activity warrants further investigations to elucidate to which extent phosphocholine contents and activation of different choline kinase isoforms (40) may act as indicators and eventually as possible pharmacodynamic markers of activation or inhibition of signaling pathways in ovarian cancer cells.

Regarding phosphatidylcholine hydrolysis pathways, we detected a five-fold activation of PLC/PLD, which likely further contributes to the accumulation of phosphocholine in ovary tumor cells. This result may open new areas of investigation, especially in view of our recent report on activation and subcellular translocation of a phosphatidylcholine-PLC isoform in mitogen-stimulated fibroblasts compared with quiescent control cells (29). Moreover, our current localization studies show that phosphatidylcholine-PLC is mainly confined to cytoplasmic compartments in EONT but becomes massively expressed on the plasma membrane of EOC cells. These investigations might shed light on the mechanisms of phosphatidylcholine-PLC activation and its role in ovarian cancer progression.

Besides addressing new questions on the relationships between phosphatidylcholine cycle and signal transduction pathways, the observed increase in choline kinase in EOC cells may provide further support to the use of [^{11}C]choline or [^{18}F]choline as radiotracers in PET examinations of primary pelvic tumors and lymph node metastases (10, 11) as an alternative to [^{18}F]fluorodeoxyglucose, whose abundant radioactivity excretion into the bladder may hamper image interpretation (45, 46). Thus, we investigated the incorporation of [^{14}C]choline in EOC and EONT cells as a model to assess the potential of choline-based PET examinations in ovary cancer diagnosis and follow-up. In our experimental approach, the scintillation counts obtained after 1-hour cell incubation with the radiolabeled substrate should mainly reflect the total amount of intracellular radiotracer that enters the cell by choline transport and accumulates, by efficient phosphorylation, in the pool of water-soluble intermediates of the Kennedy pathway (30–32, 47, 48). Furthermore, a recent analysis of internalization kinetics of a nonmetabolizable choline analogue in cancer cells clearly showed that, whereas at short incubation times (5 minutes) radiolabel internalization was largely dependent on the choline transport rate, at longer incubation times (>20 minutes) choline phosphorylation became the dominant step in cellular enrichment (49). Thus, even in the absence of detailed analyses on choline transport rates, it is likely that the 5- to 15-fold increase in [methyl-^{14}C]choline uptake in EOC compared with EONT cells is due mainly to choline kinase activation. Similar mechanisms and rates of radiolabeled choline uptake, conversion, and accumulation can be assumed to take place in PET analyses done at

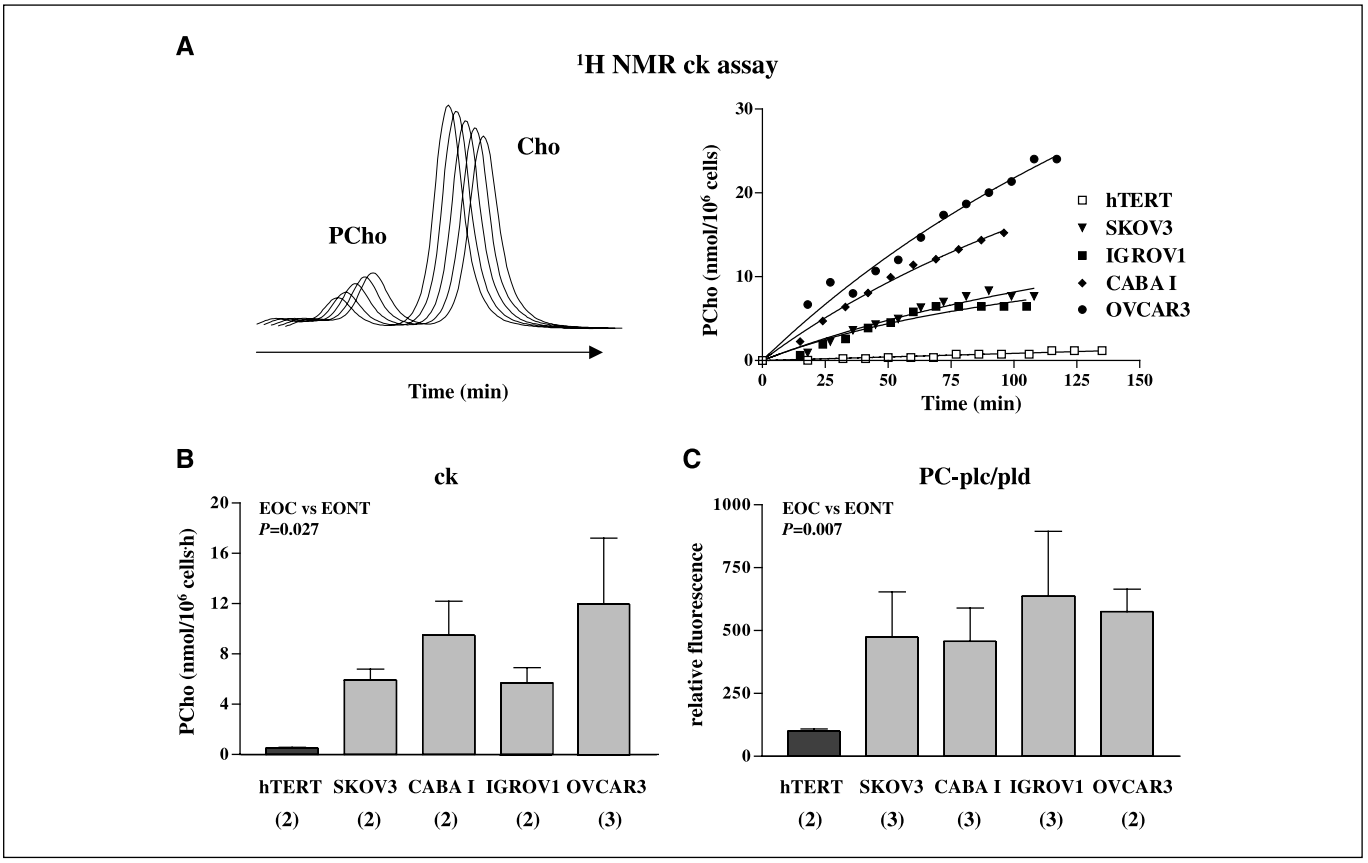

Figure 5. Basal activity rates of enzymes responsible for phosphocholine production in phosphatidylcholine biosynthetic and catabolic pathways in hTERT and EOC cells. *A,* representative ^{1}H NMR choline kinase assays done on cell cytosolic preparations by measuring the increase in NMR phosphocholine signal area at different times after addition of exogenous choline, ATP, and $MgCl_2$: *left,* simultaneous detection of phosphocholine and choline in CABA I between 15 and 65 minutes; *right,* time course of net phosphocholine production in experiments using hTERT and EOC samples. *B,* basal choline kinase activity rates determined by NMR assays. *C,* overall phosphatidylcholine-PLC/PLD activity of the same cell systems as in *B* determined by fluorimetric assays (relative resorufin fluorescence normalized to that of hTERT taken as 100). See Materials and Methods for further details. Statistical significance of differences was determined using Student's *t* tests. The number of independent experiments for each cell type is indicated in parentheses. For error bars, see legend to Fig. 3.

~1 hour after *in vivo* administration of the radiolabeled choline bolus. It should however be noted that the time window of 1 hour for PET examinations requires the use of an appropriate radiotracer, such as [^{18}F]choline (half-life, 110 minutes) rather than [^{11}C]choline (20 minutes).

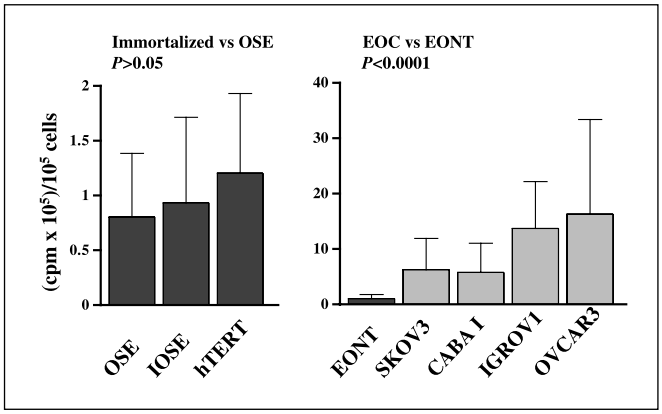

Figure 6. Uptake of [methyl-^{14}C]choline by intact EONT and EOC cells after 1-hour incubation with the radiolabeled substrate. *Columns,* mean values of four independent experiments (statistical significance evaluated by ANOVA); *bars,* SD.

Finally, the *in vitro* NMR spectral and biochemical patterns detected in the present study have qualitative similarities with those in breast cancer cells. Thus, the high-resolution and *in vivo* MRS methods already successfully applied to mammary carcinoma patients (9, 50) may well prove useful in ovary cancer patients. In particular, the here reported quantification of phosphatidylcholine metabolites in cultured EOC cell lines may provide the grounds for interpreting MRS measurements on the "choline" signal *in vivo* in terms of tumor progression, relapse, or response to therapy.

The overall body of presented data may help to elucidate aspects of EOC biology and provide a rational basis for further developing clinical noninvasive imaging methods suitable for ovary cancer diagnosis and follow-up.

Acknowledgments

Received 4/4/2005; revised 8/2/2005; accepted 8/16/2005.

Grant support: Special Project of the Italian Health Ministry 2001 and Cassa di Risparmio delle Provincie Lombarde Foundation (F. Podo and S. Canevari).

The costs of publication of this article were defrayed in part by the payment of page charges. This article must therefore be hereby marked *advertisement* in accordance with 18 U.S.C. Section 1734 solely to indicate this fact.

We thank Massimo Giannini for high-quality maintenance of NMR equipment, Alessandro Ricci for technical assistance in cell culture and NMR experiments (Istituto Superiore di Sanità), and Dr. Marco Gobbi (Istituto Mario Negri, Milan, Italy) for advice on statistical analyses.

References

1. Jemal A, Tiwari RC, Murray T, et al. Cancer statistics, 2004. CA Cancer J Clin 2004;54:8–29.
2. Ozols RF, Bookman MA, Connolly DC, et al. Focus on epithelial ovarian cancer. Cancer Cell 2004;5:19–24.
3. Balli S, Fey MF, Hanggi W, et al. Ovarian cancer. An institutional review of patterns of care, health insurance and prognosis. Eur J Cancer 2000;36:2061–8.
4. Negendank WG. Studies of human tumors by MRS: a review. NMR Biomed 1992;5:303–24.
5. de Certaines JD, Larsen VA, Podo F, Carpinelli G, Briot O, Henriksen O. *In vivo* ^{31}P MRS of experimental tumours. NMR Biomed 1993;6:345–65.
6. Podo F. Tumour phospholipid metabolism. Review article. NMR Biomed 1999;12:413–39.
7. Ackerstaff E, Glunde K, Bhujwalla ZW. Choline phospholipid metabolism: a target in cancer cells? J Cell Biochem 2003;90:525–33.
8. Kurhanewicz J, Vigneron DB, Nelson SJ. Three-dimensional magnetic resonance spectroscopic imaging of brain and prostate cancer. Neoplasia 2000;2:166–89.
9. Katz-Brull R, Lavin PT, Lenkinski RE. Clinical utility of proton magnetic resonance spectroscopy in characterizing breast lesions. J Natl Cancer Inst 2002;94:1197–203.
10. Hara T. ^{18}F-Fluorocholine: a new oncologic PET tracer. J Nucl Med 2001;42:1815–7.
11. Torizuka T, Kanno T, Futatsubashi M, et al. Imaging of gynecologic tumors: comparison of ^{11}C-choline PET with ^{18}F-FDG PET. J Nucl Med 2003;44:1051–6.
12. Aboagye EO, Bhujwalla ZM. Malignant transformation alters membrane choline phospholipid metabolism of human mammary epithelial cells. Cancer Res 1999;59:80–4.
13. Glunde K, Jie C, Bhujwalla M. Molecular causes of the aberrant choline phospholipid metabolism in breast cancer. Cancer Res 2004;64:4270–6.
14. Ackerstaff E, Pflug BR, Nelson JB, Bhujwalla ZM. Detection of increased choline compounds with proton nuclear magnetic resonance spectroscopy subsequent to malignant transformation of human prostatic epithelial cells. Cancer Res 2001;61:3599–603.
15. Okada T, Harada M, Matsuzaki K, Nishitani H, Aono T. Evaluation of female intrapelvic tumors by clinical proton MR spectroscopy. J Magn Reson Imaging 2001;13:912–7.
16. Wallace JC, Raaphorst GP, Somorjai RL, et al. Classification of ^{1}H MR spectra of biopsies from untreated and recurrent ovarian cancer using linear discriminant analysis. Magn Reson Med 1997;38:569–76.
17. Ferretti A, D'Ascenzo S, Knijn A, Iorio E, Dolo V, Podo F. Detection of polyol accumulation in a new ovarian carcinoma cell line, CABA 1: a ^{1}H NMR study. Br J Cancer 2002;86:1180–7.
18. Kruk PA, Maines-Bandiera SL, Auersperg NA. Simplified method to culture human ovarian surface epithelium. Lab Invest 1990;63:132–6.
19. Benard J, Da Silva J, De Blois MC, et al. Characterization of a human ovarian adenocarcinoma line, IGROV1, in tissue culture and in nude mice. Cancer Res 1985;45:4970–9.
20. Hamilton TC, Young RC, McKoy WM, et al. Characterization of a human ovarian carcinoma cell line (NIH:OVCAR-3) with androgen and estrogen receptors. Cancer Res 1983;43:5379–89.
21. Fogh J, Fogh JM, Orfeo T. One hundred and twenty-seven cultured human tumor cell lines producing tumors in nude mice. J Natl Cancer Inst 1977;59:221–6.
22. Bast RC, Jr., Feeney M, Lazarus H, Nadler LM, Colvin RB, Knapp RC. Reactivity of a monoclonal antibody with human ovarian carcinoma. J Clin Invest 1981;68:1331–7.
23. Dolo V, Ginestra A, Violini S, et al. Ultrastructural and phenotypic characterization of CABA I, a new human ovarian cancer cell line. Oncol Res 1997;9:129–38.
24. Granata F, Iorio E, Carpinelli G, Giannini M, Podo F. Phosphocholine and phosphoethanolamine during chick embryo myogenesis: a ^{31}P-NMR study. Biochim Biophys Acta 2000;1483:334–42.
25. Podo F, Ferretti A, Knijn A, et al. Detection of phosphatidylcholine-specific phospholipase C in NIH-3T3 fibroblasts and their H-*ras* transformants: NMR and immunochemical studies. Anticancer Res 1996;16:1399–412.
26. Proietti E, Carpinelli G, Di Vito M, Belardelli F, Gresser I, Podo F. ^{31}P-nuclear magnetic resonance analysis of interferon-induced alterations of phospholipid metabolites in interferon-sensitive and interferon-resistant Friend leukemia cell tumors in mice. Cancer Res 1986;46:2849–57.
27. Podo F, Carpinelli G, Di Vito M, et al. Nuclear magnetic resonance analysis of tumour necrosis factor-induced alterations of phospholipid metabolites and pH in Friend leukemia cell tumors and fibrosarcomas in mice. Cancer Res 1987;47:6481–9.
28. Ishidate K. Choline transport and choline kinase. In: Vance DE, editor. Phosphatidylcholine metabolism. Boca Raton: CRC Press; 1989. p. 9–32.
29. Ramoni C, Spadaro F, Barletta B, Dupuis ML, Podo F. Phosphatidylcholine-specific phospholipase C in mitogen-stimulated fibroblasts. Exp Cell Res 2004;299:370–82.
30. Vance DE, Trip EM, Paddon HB. Poliovirus increases phosphatidylcholine biosynthesis in HeLa cells by stimulation of the rate-limiting reaction catalyzed by CTP: phosphocholine cytidylyltransferase. J Biol Chem 1980;255:1064–9.
31. Warden CH, Friedkin M. Regulation of phosphatidylcholine biosynthesis by mitogenic growth factors. Biochim Biophys Acta 1984;792:270–80.
32. Yoshimoto M, Waki A, Obata A, Furukawa T, Yonekura Y, Fujibayashi Y. Radiolabeled choline as a proliferation marker: comparison with radiolabeled acetate. Nucl Med Biol 2004;31:859–65.
33. Mufson RA, Okin E, Weinstein IB. Phorbol esters stimulate the rapid release of choline from prelabelled cells. Carcinogenesis 1981;2:1095–102.
34. Glunde K, Ackerstaff E, Natarajan K, Artemov D, Bhujwalla ZM. Real-time changes in ^{1}H and ^{31}P NMR spectra of malignant human mammary epithelial cells during treatment with the anti-inflammatory agent indomethacin. Magn Reson Med 2002;48:819–25.
35. Kaye S, Gershensen D, Hung M, Seiden M. Discussion: molecular therapeutics and pharmacogenomics. Gynecol Oncol 2003;88:S93–6.
36. Steinmetz R, Wagoner HA, Zeng P, et al. Mechanisms regulating the constitutive activation of the extracellular signal-regulated kinase (ERK) signaling pathway in ovarian cancer and the effect of ribonucleic acid interference for ERK1/2 on cancer cell proliferation. Mol Endocrinol 2004;18:2570–82.
37. McDaid HM, Cairns MT, Atkinson RJ, et al. Increased expression of the RIα subunit of the cAMP-dependent protein kinase A is associated with advanced stage ovarian cancer. Br J Cancer 1999;5–6:933–9.
38. Fang X, Schummer M, Mao M, et al. Lysophosphatidic acid is a bioactive mediator in ovarian cancer. Biochim Biophys Acta 2002;1582:257–64.
39. Ramirez de Molina A, Rodriguez-Gonzalez A, Lacal JC. From Ras signalling to ChoK inhibitors: a further advance in anticancer drug design. Cancer Lett 2004;206:137–48.
40. Aoyama C, Liao H, Ishidate K. Structure and function of choline kinase isoforms in mammalian cells. Prog Lipid Res 2004;43:266–81.
41. Wieprecht M, Wieder T, Geilen CC. *N*-[2-bromocinnamyl(amino)ethyl]-5-isoquinolinesulphonamide (H-89) inhibits incorporation of choline into phosphatidylcholine via inhibition of choline kinase and has no effect on the phosphorylation of CTP:phosphocholine cytidylyltransferase. Biochem J 1994;297:241–7.
42. Bjørkøy G, Overvatn A, Diaz-Meco MT, Moscat J, Johansen T. Evidence for a bifurcation of the mitogenic signaling pathway activated by Ras and phosphatidylcholine-hydrolyzing phospholipase C. J Biol Chem 1995;270:21299–306.
43. Luquain C, Singh A, Wang L, Natarajan V, Morris AJ. Role of phospholipase D in agonist-stimulated lysophosphatidic acid synthesis by ovarian cancer cells. J Lipid Res 2003;44:1963–75.
44. Eder AM, Sasagawa T, Mao M, Aoki J, Mills GB. Constitutive and lysophosphatidic acid (LPA)-induced LPA production: role of phospholipase D and phospholipase A2. Clin Cancer Res 2000;6:2482–91.
45. Cook GJR. Oncological molecular imaging: nuclear medicine techniques. Br J Radiol 2003;76:S152–8.
46. Tian M, Zhang H, Higuchi T, Oriuchi N, Endo K. Oncological diagnosis using (11)C-choline-positron emission tomography in comparison with 2-deoxy-2-[(18)F] fluoro-D-glucose-positron emission tomography. Mol Imaging Biol 2004;6:172–9.
47. Katz-Brull R, Degani H. Kinetics of choline transport and phosphorylation in human breast cancer cells: NMR application of the zero trans method. Anticancer Res 1996;16:1375–80.
48. Vance JE, Vance DE. Phospholipid biosynthesis in mammalian cells. Biochem Cell Biol 2004;82:113–28.
49. Henriksen G, Herz M, Hauser A, Schwaiger M, Wester H-J. Synthesis and preclinical evaluation of the choline transport tracer deshydoxy-[^{18}F]fluorocholine ([^{18}F]dOC). Nucl Med Biol 2004;31:851–8.
50. Yeung DKW, Humairah SC, Gary MKT. Human breast lesions: characterization with contrast-enhanced *in vivo* proton MR spectroscopyinitial results. Radiology 2001; 220:40–6.